IEEE Access
Multidisciplinary | Rapid Review | Open Access Journal

Received May 11, 2022, accepted June 11, 2022, date of publication June 15, 2022, date of current version June 23, 2022.

Digital Object Identifier 10.1109/ACCESS.2022.3183332

An Improved Three-Level Cascaded Control for LCL-Filtered Grid-Connected Inverter in Complex Grid Impedance Condition

MIN HUANG, (Member, IEEE), ZHICHENG ZHANG, WEIMIN WU, (Member, IEEE), AND ZHILEI YAO, (Senior Member, IEEE)

Department of Electronic Engineering, Shanghai Maritime University, Shanghai 201306, China

Corresponding author: Min Huang (minhuang@shmtu.edu.cn)

This work was supported in part by the National Natural Science Foundation of China under Grant 52077131, and in part by the Shanghai Frontiers Science Center of ""Full Penetration" Far-Reaching Offshore Ocean Energy and Power."

ABSTRACT The passivity-based control (PBC) with Euler–Lagrange (EL) model has been used for LCL-filtered grid-connected converter. However, the impacts of the control delay and the interaction resonances under capacitive grid impedance are rarely considered for PBC method. Nonlinear Lyapunov's stability theory is hard to estimate the stability of the system and accurately design the controller parameters considering the control delay. This paper derived the impedance model of LCL-filtered grid-connected inverter with grid current control based on PBC method. The passive theory and the zero-pole maps are applied to reveal the influence of the digital delay and differential item of inverter current loop. A new three-level cascaded control method is then proposed based on traditional PBC method to achieve stability and high robustness in complex grid. Furthermore, controller parameters are designed accurately to maintain passivity within switching frequency ranges and parameter variations of the LCL filter are investigated. Final validation of the effectiveness and performance of the proposed control structure is performed by simulation and experimentation.

INDEX TERMS Complex grid impedance, delay, LCL-filter, passivity, robust, stability analysis.

I. INTRODUCTION

Grid-connected voltage source inverters (VSI) are widely used in distributed power generation system. Due to the switching actions of the inverters, output filters are always utilized to attenuate switching harmonics to fit grid connection requirements at the point of common coupling (PCC). Comparing to L or LC type filters, LCL type filters perform better switching harmonics attenuation ability with much smaller total inductors [1]. However, LCL filters inherent resonance issue may destroy the stability of the whole inverter system. In addition, new energy power generations are widely used in the power supply field in remote areas, where the power supply lines are long and the grid impedance could be capacitive [2], [3]. Hence, system destabilizing events may be triggered by the external interactions between the inverter and the weak grid as well as among the paralleled inverters with increasing penetration of renewable energy resources [4], [5].

The associate editor coordinating the review of this manuscript and approving it for publication was Guangya Yang.

Many scholars have proposed damping methods to solve LCL filter resonance issues [6]–[10]. Passive damping is the most straightforward approach to tackle resonance issue by inserting a dissipative resistor in series or in parallel with the LCL filter capacitor. It is extremely simple but could cause unexpected extra power loss on damping resistor and degradation of harmonic attenuation ability [11], [12]. A preferable way is to adopt active damping which design more complicated control loops feedback variables to construct virtual resistors. Despite better efficiency of conventional active damping methods such as capacitor current or capacitor voltage feedback, current weighted average, the control effects are constrained by digital control delay and grid impedance [13], [14].

Since the drawbacks of conventional linear control methods, some researchers switch their attention to a series of nonlinear control approaches. Nonlinear control strategies such as, model predictive control [15], slide mode control (SMC) [16], passivity-based control (PBC) [17]–[20], etc. perform better robustness, static and dynamic in comparison

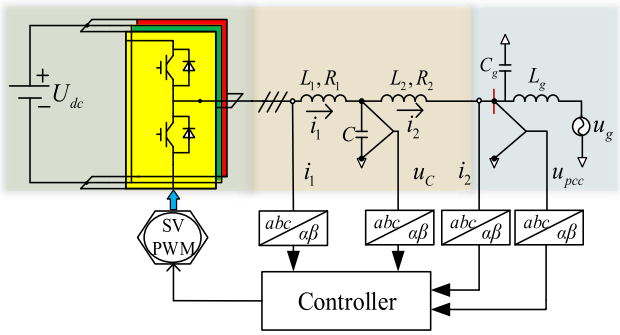

FIGURE 1. Topology of grid-connected inverter with LCL filter.

with linear control strategies due to inverters' nonlinear characteristics. However, it is hard exactly design control parameters and analyze the system stability for nonlinear control strategies, especially considering system delays and grid impedance. A linearized model for three-phase LCL-filtered grid-connected VSI with PWM-SMC control is proposed in [21] and a three loop step-by-step design method of the controller is also developed. The PBC method has clear physical meaning since the fundamentals of mathematics are based on Euler-Lagrange (EL) model to shape energy and inject damping [22]–[24]. In [25], a step-by-step parameters design method is proposed to select the damping gains of PBC controller from inside to outside to limit the steady-state error of grid-injected current for grid-connected inverter. PWM-SMC and PBC methods for LCL-filtered grid-connected VSI are similar to full state feedback controls including the feedforward control of the PCC voltage, which can provide stability and strong robustness against parameters perturbations. The PBC method has also been applied successfully to static synchronous compensator STATCOM [26] the railway power systems [27]. According to the existing literature, few scholars have examined the effects of delay and grid impedance on an LCL-filtered grid connected inverter with a PBC controller, especially in a capacitive grid or a complicated system.

In fact, the nonlinear PBC controller relies on the exact mathematic model when inject the damping to ensure the global asymptotic stability. The delay is normally not modeled in the PBC control design and stability analysis. In some cases, a rate limiter link or low pass filter is also added to the feedforward paths [28], [29]. The passivity theory has been also adopted by linear controllers by analyzing the admittance model in frequency-domain [3], [30]. Frequency domain passivity theory was introduced to guide dissipative damping selection and assess external stability of the inverter with the utilization of impedance-based model. Although this method is different from the PBC approach, it also can be used to improve the performance of PBC controller for grid-connected VSI system. Note that the passivity theory is a sufficient but not necessary stability condition. As mentioned in previous studies, the instability would arise in the case of weak grid due to the interaction between the grid impedance and the output impedance of the current-controlled inverter. The impedance-based stability analysis method has been widely utilized in recent years [30]–[33]. A number of control schemes are devoted to expand passive region, many control algorithms can realize totally passive within Nyquist frequency. However, some literature indicated that sometimes it is not enough to eliminate the risk for destabilization of poorly damped grid resonances within the Nyquist frequency, but also above, the Nyquist frequency [33].

Based on the traditional PBC control theory and the passivity theory, this paper proposed a new three-level cascaded control system for grid-connected VSC with LCL filter to solve the oscillation problem. In order to guarantee the external stability, a suitable impedance model of the proposed control is deduced by employing reasonable modeling methods. Then, the controller parameters are accurately designed for realizing passivity within switching frequency. Finally, simulation and experimental results demonstrate the effectiveness of the proposed three-level cascaded control structure and the design method of controller parameters.

II. CIRCUIT MODELING AND TRADITIONAL PBC FOR LCL-FILTERED GRID-CONNECTED INVERTER

A. CIRCUIT MODEL

The structure of a three-phase voltage-source inverter (VSI) cascades an *LCL*-type filter is shown in Fig. 1. L_1, L_2, and C are the inverter-side inductor, grid-side inductor, and filter capacitor. R_1 and R_2 represent the line resistances of L_1 and L_2, respectively, and the resistive components tend to make the system more stable. Also, L_g and C_g represents the grid inductance and grid capacitor, respectively. The grid impedance may vary over a wide range and hence a robust controller should be designed.

Moreover, the inverter-side current, grid-side current, capacitor voltage, PCC voltage and DC bus voltage are expressed by i_1, i_2, u_C, u_{pcc}, U_{dc}, respectively. For objectives of output current regulation, grid synchronization and active damping, the i_1, i_2, u_C, and u_{pcc} are sensed and fed back to the controller.

Based on the symbols defined in Fig.1, the three-phase VSI with an LCL-type filter can be expressed as follows in alpha-beta coordinate:

$$\begin{cases} L_1 \dfrac{di_{1k}}{dt} + R_1 i_{1k} + u_{Ck} = u_k \\ C \dfrac{du_{Ck}}{dt} + i_{2k} - i_{1k} = 0 \\ L_2 \dfrac{di_{2k}}{dt} + R_2 i_{2k} - u_{Ck} = -u_{pcck}, \end{cases} \quad (k = \alpha, \beta) \qquad (1)$$

where u_k is the voltage of the inverter side. For three-phase inverter, the controller design for α-axis and the β-axis components are same and independent to each other. The following part will focus on the α-axis and omit the subscripts "α, β" in order to simplify the description.

From the (1), the EL model of the three-phase VSI with LCL-type filter can be expressed as

$$\boldsymbol{M}\dot{\boldsymbol{x}} + \boldsymbol{J}\boldsymbol{x} + \boldsymbol{R}\boldsymbol{x} = \boldsymbol{U} \tag{2}$$

where $\boldsymbol{M}, \boldsymbol{J}, \boldsymbol{R}, \boldsymbol{x}$ are described as

$$\boldsymbol{M} = \begin{bmatrix} L_1 & 0 & 0 \\ 0 & C & 0 \\ 0 & 0 & L_2 \end{bmatrix}, \quad \boldsymbol{J} = \begin{bmatrix} 0 & 1 & 0 \\ -1 & 0 & 1 \\ 0 & -1 & 0 \end{bmatrix} \tag{3}$$

$$\boldsymbol{R} = \begin{bmatrix} R_1 & 0 & 0 \\ 0 & 0 & 0 \\ 0 & 0 & R_2 \end{bmatrix}, \quad \boldsymbol{x} = \begin{bmatrix} i_1 \\ u_C \\ i_2 \end{bmatrix}, \quad \boldsymbol{U} = \begin{bmatrix} u \\ 0 \\ u_{pcc} \end{bmatrix} \tag{4}$$

$\boldsymbol{M}$ is the positive definite inertial matrix and $\boldsymbol{M} = \boldsymbol{M}^T$; $\boldsymbol{J}$ is the antisymmetric interconnection matrix and $\boldsymbol{J} = -\boldsymbol{J}^T$; $\boldsymbol{R}$ is the positive definite symmetric matrix which denote the dissipation characteristic of the system, and $\boldsymbol{U}$ is the external input matrix which represents the energy exchange between surroundings and the system.

B. TRADITIONAL PASSIVITY-BASED CONTROL DESIGN PROCEDURE

Step 1: Define error dynamic

The error dynamics are the key to design globally asymptotically stable and zero steady-state error controller. The error system of VSI system can be defined as:

$$\boldsymbol{x}_e = \boldsymbol{x}^* - \boldsymbol{x} \tag{5}$$

where $\boldsymbol{x}^*$ is the desired stable equilibrium point of the VSI system and $\boldsymbol{x}_e$ is dynamic error.

Step 2: Inject damping to accelerate dissipation

In order to accelerate the speed of the $\boldsymbol{x}_e$ convergence to zero, a damping matrix $\boldsymbol{R}_d$ can be added to the error system.

$$\boldsymbol{R}_{new} = \boldsymbol{R} + \boldsymbol{R}_d \tag{6}$$

where $\boldsymbol{R}_d = diag[r_1, r_2, r_3]$, and $r_1 > 0, r_2 > 0, r_3 > 0$.

Step 3: Deduce control law

Substitution (5) into (2), the new error equation can be obtained in (7). $\boldsymbol{J}\boldsymbol{x}_e$ is used to eliminate the coupling terms of system.

$$\begin{aligned} \boldsymbol{M}\dot{\boldsymbol{x}}_e + \boldsymbol{J}\boldsymbol{x}_e + \boldsymbol{R}_{new}\boldsymbol{x}_e &= \boldsymbol{M}\dot{\boldsymbol{x}}^* + \boldsymbol{J}\boldsymbol{x}^* + \boldsymbol{R}\boldsymbol{x}^* + \boldsymbol{R}_d\boldsymbol{x}_e - \boldsymbol{U} \\ &= \boldsymbol{J}\boldsymbol{x}_e \end{aligned} \tag{7}$$

In analog control system, time delay is assumed as zero. When error dynamic $\boldsymbol{x}_e$ converges to 0, the final control law will be written as,

$$\boldsymbol{U} = \boldsymbol{M}\dot{\boldsymbol{x}}^* + \boldsymbol{J}\boldsymbol{x} + \boldsymbol{R}\boldsymbol{x}^* + \boldsymbol{R}_d\boldsymbol{x}_e \tag{8}$$

Step 4: Analyze stability

According to the Lyapunov's stability criterion, the positive definite of the energy function of the error $\boldsymbol{H}_e$ and the negative definite of its derivative $\dot{\boldsymbol{H}}_e$ can be found, which satisfies the asymptotic stability.

$$\begin{cases} \boldsymbol{H}_e = \dfrac{1}{2}\boldsymbol{x}_e^T\boldsymbol{M}\boldsymbol{x}_e > 0 \\ \dot{\boldsymbol{H}}_e = \boldsymbol{x}_e^T\boldsymbol{M}\dot{\boldsymbol{x}}_e = -\boldsymbol{x}_e^T(\boldsymbol{R}_{new}\boldsymbol{x}_e) < 0 \end{cases} \tag{9}$$

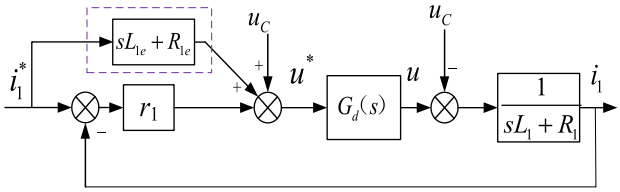

FIGURE 2. Diagram of inverter side control loop.

C. PASSIVITY-BASED CONTROL CONSIDERING DIGITAL IMPLEMENTION

Compared to analog control system, digital control method normally incorporates time delay of 1.5 T, which is caused by the pulse width modulator and controller, while T represents the sampling period [33]. However, a pure delay model is imprecise for the study of the above-Nyquist-frequency properties. In this paper, pulse width modulator is presented by a zero-order-hold (ZOH) model rather than a pure delay model, as shown in (10). The ZOH model in s-domain is expressed as

$$G_{ZOH}(s) = e^{-0.5Ts}\frac{\sin(\omega T/2)}{\omega T/2} \tag{10}$$

Then, total delay is written as follows:

$$G_d(s) = e^{-1.5Ts}\frac{2\sin(\omega T/2)}{\omega T} \tag{11}$$

It should be noted that the complex frequency domain "s" is neglected in the following analysis to simplify the expressions. For example, $G_d(s)$ is written as G_d. The delay is varying with frequency of trigonometric function. The updated control law can be deduced in the following

$$u = G_d.u^* \tag{12}$$

where u^* represents the ideal control law signal and u is the real control drive signal.

For the inner loop, as shown in Fig.2, u is not equal to u^* under the condition of time delay, therefore, Lyapunov's stability criterion is hard to assess the stability of traditional passivity-based control considering the control delay. The time-delay is directly added to the inverter side current inner loop but indirectly to the capacitor voltage loop and the grid side current loop, which has the most greatest and direct impact on the inverter side current loop. In Ref. [28], amplitude limiting output has been carried out for all differential terms with good results, but the amplitude limiting output is difficult to accurately build model. However, there is no reference mention the reason that amplitude limiting output or low pass filter should be added in the PBC structure. In the next part, equivalent inverter output admittance and closed-loop zero-poles of the system are derived to analyze the influence of the time delay and verify the proposed controller.

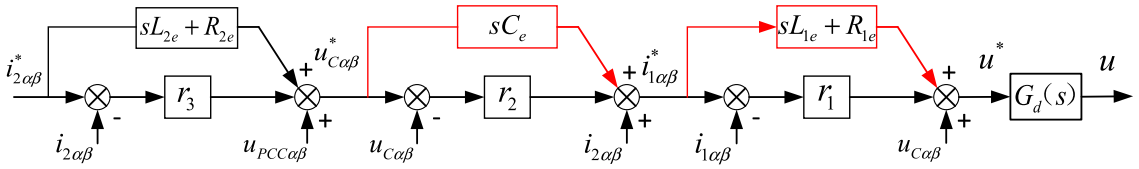

FIGURE 3. Controller structure based on traditional passive-based control.

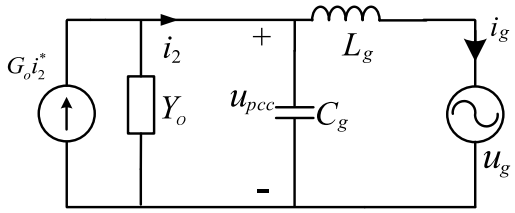

FIGURE 4. Equivalent output admittance with grid impedance.

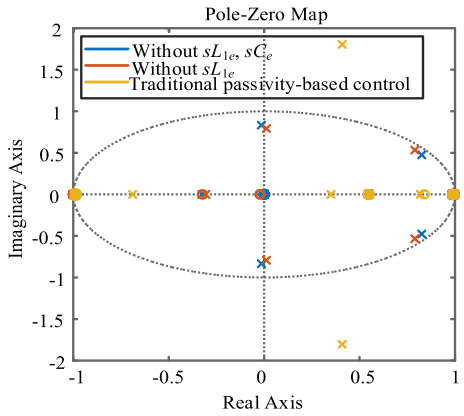

FIGURE 5. Impact of differential terms on closed-loop pole distribution.

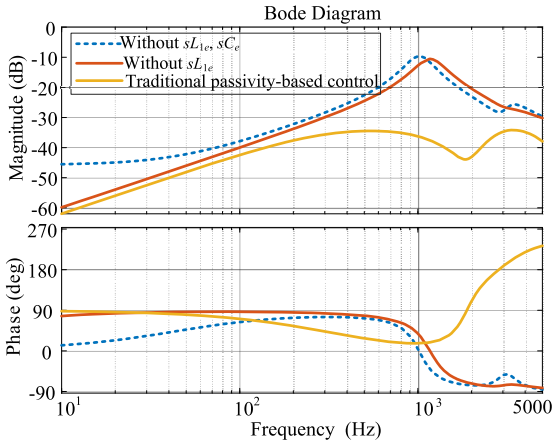

FIGURE 6. Impact of differential terms on equivalent inverter output admittance within Nyquist frequency considering time delay.

III. STABILITY ANALYSIS AND MODIFIED CONTROLLER

A. IMPEDANCE MODELLING

The LCL-filtered grid-connected inverter system can be described in Laplace domain equations, as follows

$$\begin{cases} i_2 = Au_C - Au_{pcc}, & A = 1/(sL_2 + R_2) \\ u_C = Bi_1 - Bi_2, & B = 1/(sC) \\ i_1 = Du - Du_C, & D = 1/(sL_1 + R_1) \end{cases} \tag{13}$$

The standard traditional passivity-based control approach for LCL-filtered grid-connected inverter in Laplace domain equations can be written as

$$\begin{cases} u^* = Ei_1^* - r_1 i_1 + u_C, & E = r_1 + sL_{1e} + R_{1e} \\ i_1^* = Fu_C^* - r_2 u_C + i_2, & F = r_2 + sC_e \\ u_C^* = Gi_2^* - r_3 i_2 + u_{pcc}, & G = sL_{2e} + R_{2e} + r_3 \end{cases} \tag{14}$$

where superscript "*" stands for the desired equilibrium.

Combining (13) and (14), the block diagram of the grid-side current control based on traditional PBC can be drawn in Fig.3. It can be seen as a three-level cascaded control with inverter side current loop, capacitor voltage loop and grid side current loop, including three feedforward differential terms.

Then, inverter side closed-loop expressions can be described as follows

$$i_1 = Xi_1^* - Yu_C \tag{15}$$

$$X = \frac{DEG_d}{(1 + r_1 DG_d)}, \quad Y = \frac{D(1 - G_d)}{(1 + r_1 DG_d)} u_C \tag{16}$$

Similarly, capacitor voltage closed-loop can be derived as

$$\begin{aligned} &(1 - DEG_d + r_3 DG_d)\, i_1 \\ &= DEG_d F u_C^* - \left(r_2 DEG_d - D(G_d - 1) + \frac{DEG_d}{B} \right) u_C \end{aligned} \tag{17}$$

And the admittance model for grid side current control loop is expressed as follows:

$$\begin{aligned} i_2 = &\frac{XBFG}{\left[(1 - BY + Br_2 X)A^{-1} + (XBFr_3 + B - XB)\right]} i_2^* \\ &- \frac{1 - BY + Br_2 X - XBF}{\left[(1 - BY + Br_2 X)A^{-1} + (XBFr_3 + B - XB)\right]} \\ &\times u_{pcc} \end{aligned} \tag{18}$$

The admittance model consists of closed-loop transfer function of grid side current control and inverter equivalent output admittance, which are expressed as G_o and Y_o, respectively. The corresponding schematic diagram of admittance model is shown in Fig.4, where L_g and C_g are grid impedance. Based on the passive theory [32], the interaction stability with power grid can be analyzed by inverter output admittance in frequency domain. The internal stability of LCL-filtered inverter can be assessed by closed-loop transfer function.

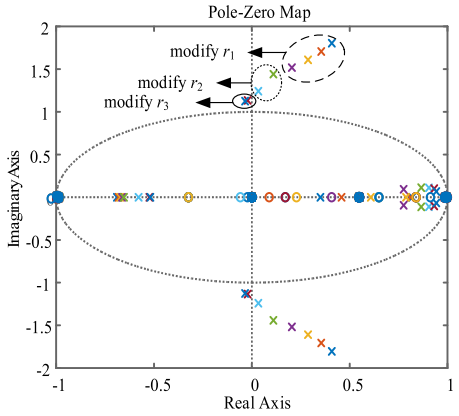

FIGURE 7. Traditional passivity-based control with modified damping gains.

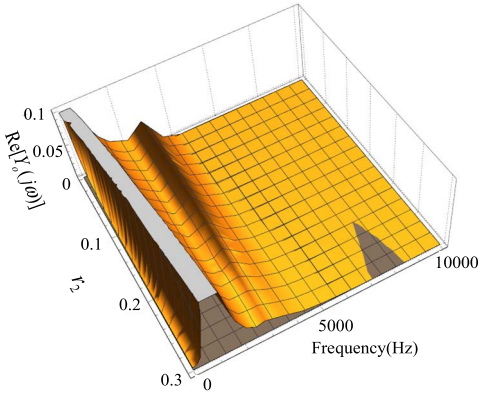

FIGURE 8. Real part of closed-loop equivalent output admittance when $r_3 = 15$.

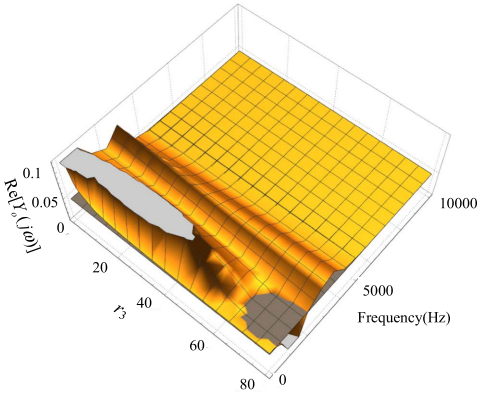

FIGURE 9. Real part of closed-loop equivalent output admittance when $r_2 = 0.1$.

B. INFLUENCE OF TIME DELAY ON DIFFERENTIAL TERMS OF PASSIVITY-BASED CONTROL

It is vital to check how the differential terms of passivity-based control impact stability of close-loop system and passivity of output admittance for LCL-filtered inverter with PBC. The circuit parameters are listed in Table 1. Fig.5 shows the closed-loop poles maps with selected controller

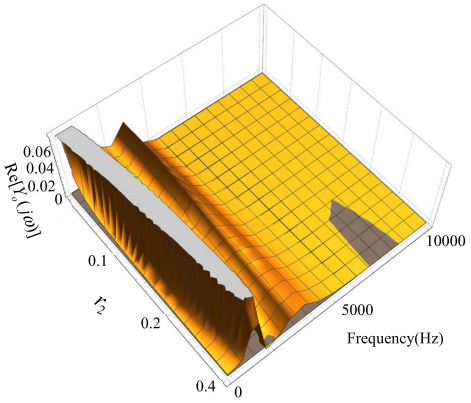

FIGURE 10. Real part of closed-loop equivalent output admittance, when $r_3 = 25$.

TABLE 1. Circuit parameters.

parameters	value
DC source voltage	U_{dc}=350V
Switch frequency	f_s=10000Hz
Sampling frequency	f=10000Hz
LCL filter parameter	L_1=1.2mH, R_1=0.1 Ω , L_2=1.2mH
	R_2=0.1 Ω , C=6μF
AC source RMS voltage	u_g=110V
AC source frequency	50Hz

parameters, $r_1 = 2$, $r_2 = 0.2$, $r_3 = 25$, considering time delay. It indicates that system is not stable with traditional PBC. When the differential term of the inverter side current loop of E is deleted, the closed-loop poles move inside the unit circle. The differential term of capacitor loop minimally influence the system stability.

From the inverter equivalent output admittance of Fig.6, it shows that the traditional PBC has non-passive regions and output admittance phase angle is out of the $[-90°, 90°]$ and greater than 180°. It also implied that the differential item of inverter side current loop will cause instability. In fact, the zero-pole distribution and inverter output admittance for the case without sL_{1e}, sC_e are almost consistent with the case when all differential terms are deleted.

It can be seen from Fig.5 and Fig.6 that the differential term of inverter side current loop will bring instability for the system. In order to exclude the particularity of parameters, as shown in Fig.7, we try to modify r_1, r_2, r_3 to make poles in unit circle. At beginning, $r_1 = 2$, $r_2 = 0.2$, $r_3 = 25$, then, the poles all move toward center of a circle when reducing r_1, r_2 and r_3, but the poles are still outside the unit circle. If all damping parameters go to zero, the controller will fail. Hence, this paper proposed a new control structure with removed differential term of inverter side current loop to improve the stability and also removed differential term of capacitor voltage loop to improve low frequency response.

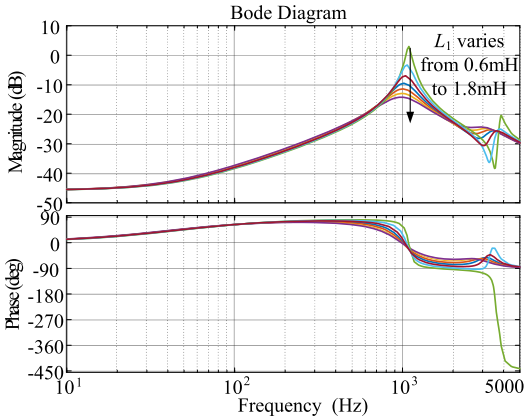

FIGURE 11. Equivalent inverter output admittance when parameter L_1 drifted.

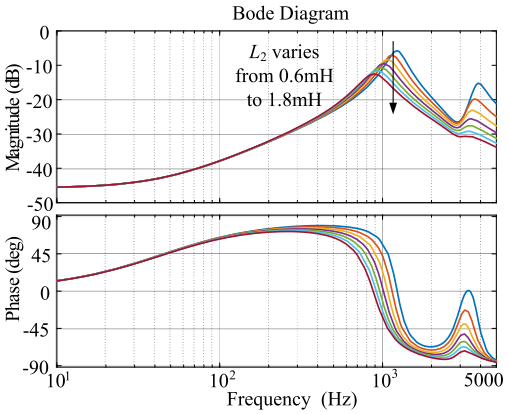

FIGURE 12. Equivalent inverter output admittance when parameter L_2 drifted.

C. CONTROLLER PARAMETERS DESIGN PROCEDURE

To design the damping gains of r_1, r_2 and r_3 of the proposed controller, the inner loop should be designed first. The time delay is approximated as first order inertial link to simplify the design process when designing the inner loop parameters, so the inner loop transfer function can be regarded as a second-order system.

In order to achieve the fastest response, the inner loop parameters are designed according to the critical damping ratio. The time required for the system to reach equilibrium from motion is the shortest under critical damping condition.

Then the inverter side current can be expressed as,

$$\begin{aligned} i_1 &= \frac{R_{1e}+r_1}{(1.5Ts+1)(sL_1+R_1)+r_1} i_1^* \\ &= \frac{\frac{r_1+R_{1e}}{1.5TL_1}}{s^2+\frac{1.5TR_1+L_1}{1.5TL_1}s+\frac{R_1+r_1}{1.5TL_1}} i_1^* \end{aligned} \tag{19}$$

When the critical damping ratio ξ is set as 1, r_1 can be calculated

$$r_1 = \frac{(1.5TR_1+L_1)^2}{6\xi^2 TL_1} - R_1 \approx 2 \tag{20}$$

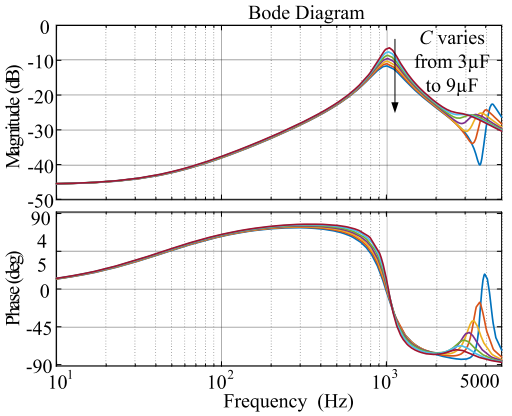

FIGURE 13. Equivalent inverter output admittance when parameter C drifted.

According to passive theory [3], the parameters r_1 and r_2 will be designed based on the inverter output admittance to eliminate the possibility of interactive resonance with grid. In addition, if its output admittance is passive in the whole frequency band, its resonance can be suppressed, which means that its interior is also stable. In fact, this can be verified by the closed-loop transfer function.

The passivity of $Y_o(s)$ in complex frequency domain can be judged by whether the real part in frequency domain Re$[Y(j\omega)]$ is greater than zero. If Re$[Y(j\omega)] > 0$, it represents the inverter system is passive. The delay G_d in $Y_o(s)$ is expanded by Euler formula and transformed into $Y_o(j\omega)$.

In this process, Wolfram Mathematics is used to calculate Re $[Y_o(j\omega)]$. In the calculation process, r_1 has been selected according to the critical damping ratio. r_2 and r_3 are two variables, designed by the value of the real part. This is a multivariable optimization problem and some iterative algorithms can be used, but the process is too cumbersome. So, this paper manually selects and iterates several groups of parameters.

Step 1: assume a value of r_1;

Step 2: calculate the feasible range of r_2 according to the selected value of r_2;

Step 3: select value of r_2 from the calculated range, then find the feasible range of r_3, and select the appropriate value of r_3, generally, the midpoint;

Step4: repeat *step* 2 and *step* 3.

After several times of cross selection, the values of r_3 and r_2 can finally be selected.

Fig.8 shows the relationship between the frequency, the range of r_2 and real part of equivalent output admittance with $r_3 = 15$. When the value of r_2 is within [0, 0.2], and the value of the real part is greater than zero within the switching frequency, which meets the requirements of passivity. Therefore, the middle value, $r_2 = 0.1$, can be chosen. In Fig.9, when r_2 is 0.1, r_3 should be greater than zero in [0, 60] to meet the requirements of passivity. Fig.10 shows the selected range of r_2. When $r_3 = 25$, r_2 can be selected from [0, 0.2]. For the closed-loop system, the inner loop is usually required to have faster bandwidth and reach

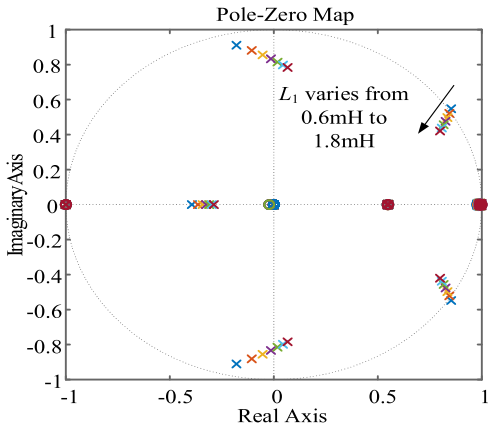

FIGURE 14. System closed-loop poles when parameter L_1 drifted.

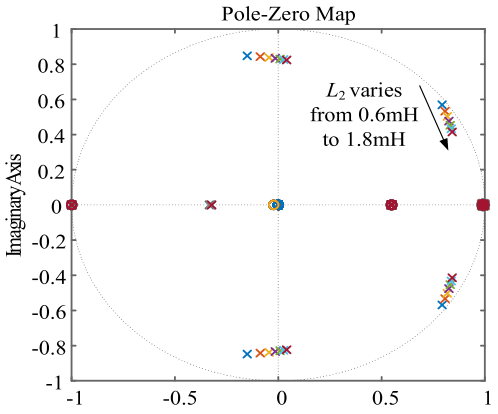

FIGURE 15. System closed-loop poles when parameter L_2 drifted.

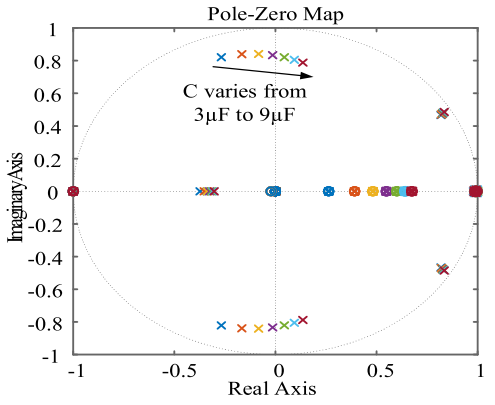

FIGURE 16. System closed-loop poles when parameter C drifted.

faster dynamic response, so $r_2 = 0.2$ is the maximum value that can be selected. Here, $r_1 = 2$, $r_2 = 0.2$ and $r_3 = 25$ are selected for the following analysis and verifications.

D. ROBUTNESS ANALYSIS

In the actual operation, the inductor and capacitor of the LCL-filter could get aging over time. Hence, the values of LCL-filter will drift in a range. Fig.11, Fig.12 and Fig.13 show equivalent inverter output admittance passivity within

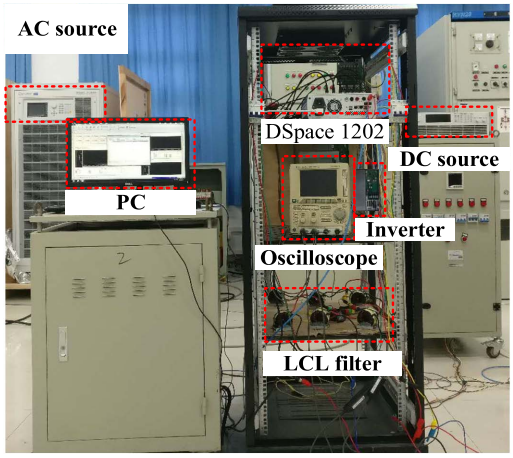

FIGURE 17. Experimental setup.

Nyquist frequency when L_1, L_2 and C vary from 50% to 150%, respectively. In Fig.11, L_1 varies from 0.6mH to 1.8mH increased by 0.2mH and the inverter output admittance is passive except the case that L_1 is 0.6mH; In Fig.12, when L_2 varies from 0.6mH to 1.8mH increased by 0.2mH, the inverter output admittance always keep passive. In Fig.13, when C varies from 3μF to 9μF increased by 1μF, the inverter output admittance can also keep passive.

Similarly, the impact of circuit parameter variations on system closed-loop stability are explored by pole-zero maps when L_1, L_2 and C vary from 50% to 150%, as shown in Fig.14, Fig.15 and Fig.16.

Fig.14 shows L_1 varies from 0.6mH to 1.8mH increased by 0.2mH and the closed-loop system keep stable except the case $L_1 = 0.6$mH; In Fig.15, L_2 varies from 0.6mH to 1.8mH increased by 0.2mH and the closed-loop system always keep stable; In Fig.16, C varies from 3μF to 9μF increased by 1μF and the closed-loop system still keep stable.

Based on the analysis of the output admittance and closed-loop zero-pole map, the passivity and stability have consistent performance for circuit parameters variations. The inverter side inductor, L_1, is the main factor for system stability and passivity. The system will turn unstable if L_1 is reduced more than 33%. When C and L_2 vary from 50% to 150%, the system is still robust to the mismatched parameters. It can be explained from another aspect that the time delay directly influence inverter current loop.

IV. SIMULATION AND EXPERIMENTAL RESULTS

In this section, a modified three-level cascaded controller based on traditional PBC for VSI with LCL filter was verified through Matlab/Simulink. To further verify the controller design and passivity analysis, in this section, an experimental prototype of VSI with LCL filter is also built, as shown in Fig. 17. The Danfoss-FC32o is powered by a DC power supply (Chroma 62150H-600S). The programmable three-phase ac source (Chroma 61830) is used to simulate the grid. The control system is implemented with a dSPACE

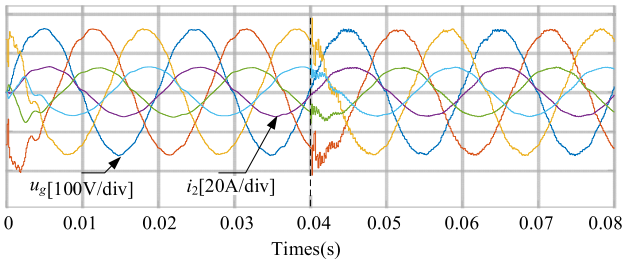

FIGURE 18. Simulation results with proposed method when grid impedance changes from $L_g = 0$, $C_g = 0$ to $L_g = 3.6$mH, $C_g = 0$.

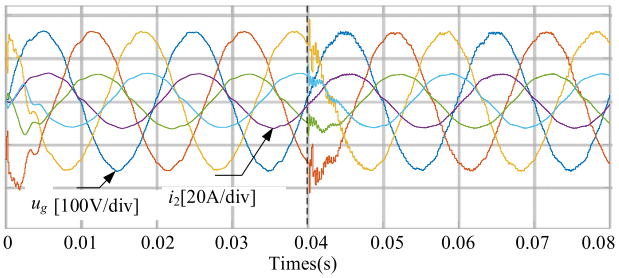

FIGURE 19. Simulation results with proposed method when grid impedance changes from $L_g = 3.6$mH, $C_g = 0$ to $L_g = 3.6$mH, $C_g = 4$ μF.

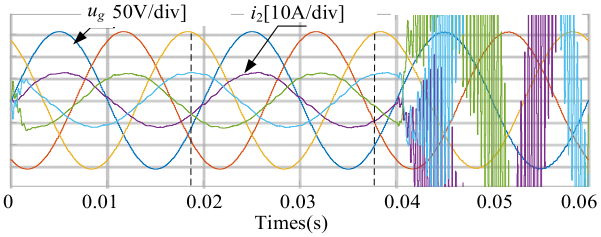

FIGURE 20. Stability verification with different controllers when $L_g = 3.6$mH, $C_g = 4\mu$F.

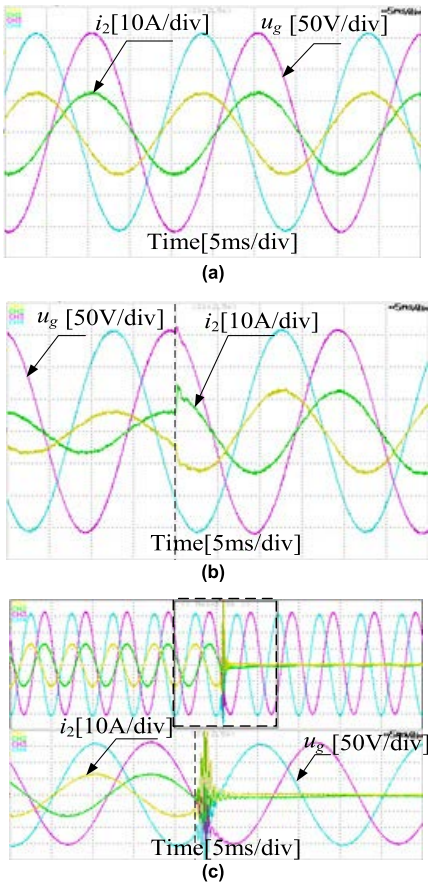

FIGURE 21. Experimental results under (a) steady state, (b) reference current steps, and (c) different control strategies when the grid $L_g = 0$ and $C_g = 0$.

DS1202 system. The grid side damping parameter r_1 is replaced by proportional resonant controller, $K_p = r_1$, $K_r = 1000$ to achieve zero steady error. The system parameters of simulation and experiments are given in Table 1.

A. SIMULATION RESULTS

Fig.18 shows the simulation results of grid current and grid voltage when $L_g = 0$ and $C_g = 0$ during 0-0.04s. At 0.04s, L_g is changed to 3.6mH and the result shows that the modified three-level cascaded control can keep system stable in inductive impedance grid. In Fig.19, grid impedance $L_g = 3.6$mH and $C_g = 0$ at beginning, then C_g is changed to 4μF at 0.04s. It can be seen that even in a complex grid impedance condition the proposed method can still work well.

Fig.20 shows the simulation results of different control structures when $L_g = 3.6$mH, $C_g = 4\mu$F. At 0s, the system is operated under proposed controller (without sL_{1e} and sC_e), then the sC_e item is added to the capacitor voltage loop. It can be seen that the system can keep stable in both cases. At 0.04s, the system turns to instable when the traditional passivity-based control is enabled (sL_{1e} is added). It verified that the differential term of the inverter side current loop in the traditional PBC will bring instability to the system.

B. EXPERIMENTAL RESULTS

To further demonstrate the validity of the proposed three-level cascaded control method and stability analysis, experimental results are carried out into ideal grid and complex grid conditions, separately. Fig. 21 presents the results of the system when the grid impedance $L_g = 0$ and $C_g = 0$. It can be seen in Fig. 21(a) that grid voltage and grid current waveforms are sinusoidal and smooth under steady state. The THD of the injected current is 1.9%. Fig. 21(b) shows the transient results when the reference value of the grid current i_2 steps from 6.4A to 12.8A. It shows that the grid current can respond quickly with the proposed three-level cascaded control structure. Furthermore, the influence of the differential item of inverter side current loop is also verified in Fig. 21(c). When the controller is suddenly switched to traditional PBC method, the system immediately turns out to be unstable and protected.

To verify the effectivity of the designed control parameters and robustness of proposed control method, Fig. 22-Fig.24

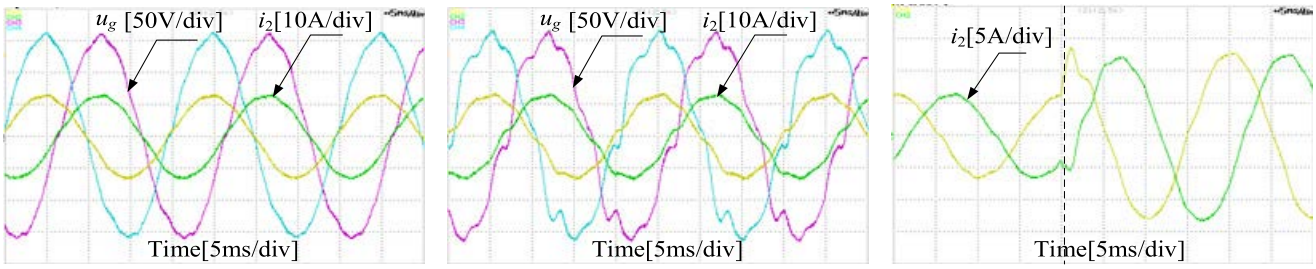

FIGURE 22. Experimental results under (a) steady state, (b) grid Distortions, and (c) reference current steps when the grid impedance $L_g = 6$mH.

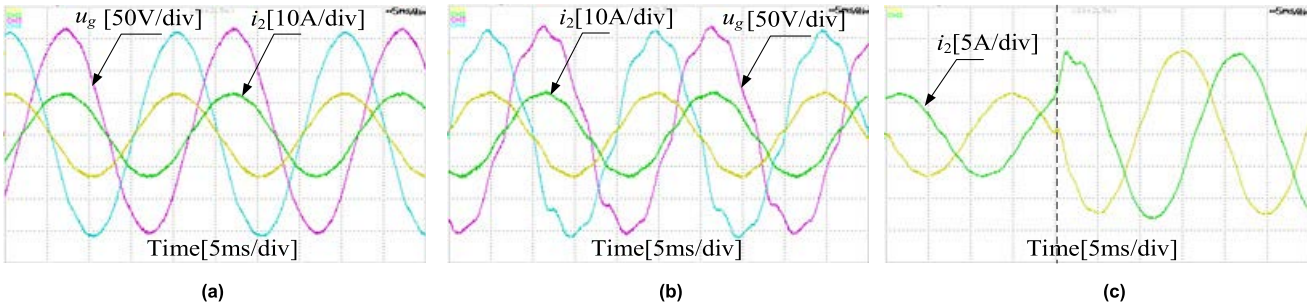

FIGURE 23. Experimental results under (a) steady state, (b) grid Distortions, and (c) reference current steps when the grid impedance $L_g = 3.6$mH and $C_g = 3\mu$F.

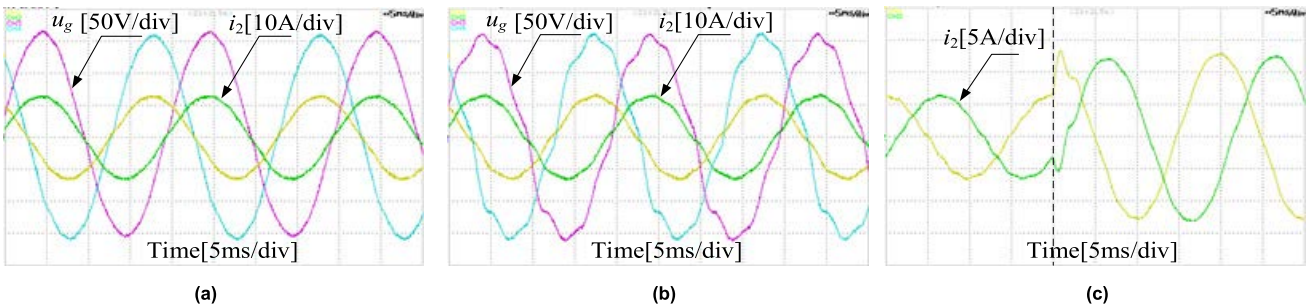

FIGURE 24. Experimental results under (a) steady state, (b) grid Distortions, and (c) reference current steps when the grid impedance $L_g = 3.6$mH and $C_g = 1\mu$F.

show detailed experimental results under different complex grid. In Fig.22, the system is operated under inductive grid with $L_g = 6$mH. The grid current quality is good and the THD is 3.1% under the steady state. Even the grid voltages are distorted by 3% of third, fifth, seventh, and ninth harmonics, the injected grid current is still sinusoidal with 4.2% of THD. Fig.22(c) shows the transient waveforms of grid currents when the grid reference current steps under the weak grid. Compared the case under the ideal grid, the overshooting is bigger and the regulation time is longer, but transient response is still very good.

Fig. 23 and Fig.24 present the performance of the system under complex grid impedance with $L_g = 3.6$mH, $C_g = 3\mu$F and $L_g = 3.6$mH, $C_g = 1\mu$F, respectively. Different L_g and C_g will result in different points of interaction between inverter output impedance and grid impedance.

In both inductive and capacitive grid impedance cases, the proposed control strategy can achieve high quality injected current and fast dynamic response under steady state and transient state. The THDs of grid currents are 2.2% and 2.1% in Fig. 23(a) and Fig. 24(a). Even under the distortion grid, the grid current can still satisfy the standard for injected current, with THDs of 4.6% and 4.4%. Hence, with proposed control structure and parameters design procedure, the LCL-filtered grid-connected inverter system can reach fast dynamic response, high stability and also robustness.

V. CONCLUSION

Traditional PBC for LCL-filtered grid-connected converter based on EL model has made good success. If the influence of time-delay is considered, the traditional nonlinear analysis approach is inaccurate. Some researchers agree that

differential term could amplify noise, and then limiters and low pass filters are used in differential terms output of PBC block to obtain good results. In fact, by analyzing closed-loop transfer function and inverter output admittance of the system, it can be found that not all differential terms affect stability. The differential term of the inverter side current loop structure is directly influenced by time delay during the discretization and the energy function is no longer accurate. This paper proposed an improved three-level cascaded structure based on traditional PBC method for LCL-filtered grid-connected inverter. A new design procedure for controller parameters is also proposed based on passivity theory with output admittance. With selected control parameters, the system can achieve passivity within switching frequency. Hence, interactive resonances with grid impedance can be avoided. The effectiveness and performance of the proposed method are verified and compared based on simulation and experimental results.

REFERENCES

[1] M. Liserre, F. Blaabjerg, and S. Hansen, "Design and control of an LCL-filter-based three-phase active rectifier," *IEEE Trans. Ind. Appl.*, vol. 41, no. 5, pp. 1281–1291, Sep. 2005.

[2] C. Xie, K. Li, J. Zou, and J. M. Guerrero, "Passivity-based stabilization of LCL-type grid-connected inverters via a general admittance model," *IEEE Trans. Power Electron.*, vol. 35, no. 6, pp. 6636–6648, Jun. 2020.

[3] X. Wang, F. Blaabjerg, and P. C. Loh, "Passivity-based stability analysis and damping injection for multiparalleled VSCs with LCL filters," *IEEE Trans. Power Electron.*, vol. 32, no. 11, pp. 8922–8935, Nov. 2017.

[4] D. Pan, X. Ruan, C. Bao, W. Li, and X. Wang, "Optimized controller design for LCL-type grid-connected inverter to achieve high robustness against grid-impedance variation," *IEEE Trans. Ind. Electron.*, vol. 62, no. 3, pp. 1537–1547, Mar. 2015.

[5] L. Harnefors, R. Finger, X. Wang, H. Bai, and F. Blaabjerg, "VSC input-admittance modeling and analysis above the Nyquist frequency for passivity-based stability assessment," *IEEE Trans. Ind. Electron.*, vol. 64, no. 8, pp. 6362–6370, Aug. 2017.

[6] H.-S. Kim and S.-K. Sul, "Resonance suppression method for grid-connected converter with LCL filter under discontinuous PWM," *IEEE Access*, vol. 9, pp. 124519–124529, 2021.

[7] M. Huang, X. Wang, P. C. Loh, and F. Blaabjerg, "Active damping of LLCL filter resonance based on LC-trap voltage or current feedback," *IEEE Trans. Power Electron.*, vol. 31, no. 3, pp. 2337–2346, Mar. 2016.

[8] W. Yao, Y. Yang, X. Zhang, F. Blaabjerg, and P. C. Loh, "Design and analysis of robust active damping for LCL filters using digital notch filters," *IEEE Trans. Power Electron.*, vol. 32, no. 3, pp. 2360–2375, Mar. 2017.

[9] Y. He, X. Wang, X. Ruan, D. Pan, X. Xu, and F. Liu, "Capacitor-current proportional-integral positive feedback active damping for LCL-type grid-connected inverter to achieve high robustness against grid impedance variation," *IEEE Trans. Power Electron.*, vol. 34, no. 12, pp. 12423–12436, Dec. 2019.

[10] L. Jia, X. Ruan, W. Zhao, Z. Lin, and X. Wang, "An adaptive active damper for improving the stability of grid-connected inverters under weak grid," *IEEE Trans. Power Electron.*, vol. 33, no. 11, pp. 9561–9574, Nov. 2018.

[11] Y. Han, M. Yang, H. Li, P. Yang, L. Xu, E. A. A. Coelho, and J. M. Guerrero, "Modeling and stability analysis of LCL-type grid-connected inverters: A comprehensive overview," *IEEE Access*, vol. 7, pp. 114975–115001, 2019.

[12] J. Ye, A. Shen, Z. Zhang, J. Xu, and F. Wu, "Systematic design of the hybrid damping method for three-phase inverters with high-order filters," *IEEE Trans. Power Electron.*, vol. 33, no. 6, pp. 4944–4956, Jun. 2018.

[13] C. Zou, B. Liu, S. Duan, and R. Li, "Influence of delay on system stability and delay optimization of grid-connected inverters with LCL filter," *IEEE Trans. Ind. Informat.*, vol. 10, no. 3, pp. 1775–1784, Aug. 2014.

[14] M. B. Said-Romdhane, M. W. Naouar, I. Slama-Belkhodja, and E. Monmasson, "Robust active damping methods for LCL filter-based grid-connected converters," *IEEE Trans. Power Electron.*, vol. 32, no. 9, pp. 6739–6750, Sep. 2017.

[15] X. Chen, W. Wu, N. Gao, H. S.-H. Chung, M. Liserre, and F. Blaabjerg, "Finite control set model predictive control for LCL-filtered grid-tied inverter with minimum sensors," *IEEE Trans. Ind. Electron.*, vol. 67, no. 12, pp. 9980–9990, Dec. 2020.

[16] H. Komurcugil, S. Ozdemir, I. Sefa, N. Altin, and O. Kukrer, "Sliding mode control for single-phase grid-connected LCL-filtered VSI with double-band hysteresis scheme," *IEEE Trans. Ind. Electron.*, vol. 63, no. 2, pp. 864–873, Feb. 2016.

[17] F. Zheng, W. Wu, B. Chen, and E. Koutroulis, "An optimized parameter design method for passivity-based control in a LCL-filtered grid-connected inverter," *IEEE Access*, vol. 8, pp. 189878–189890, 2020.

[18] S. Pang, B. Nahid-Mobarakeh, S. Pierfederici, Y. Huangfu, G. Luo, and F. Gao, "Toward stabilization of constant power loads using IDA-PBC for cascaded LC filter DC/DC converters," *IEEE J. Emerg. Sel. Topics Power Electron.*, vol. 9, no. 2, pp. 1302–1314, Apr. 2021.

[19] J. Wang, X. Mu, and K. Li, "Study of passivity based decoupling control of T-NPC PV grid connected inverter," *IEEE Trans. Ind. Electron.*, vol. 64, no. 9, pp. 7542–7551, Mar. 2017.

[20] O. Montoya, W. Gil-Gonzalez, and A. Garces, "Distributed energy resources integration in single-phase microgrids: An application of IDA-PBC and PI-PBC approaches," *Int. J. Electr. Power Energy Syst.*, vol. 112, pp. 221–231, Nov. 2019.

[21] H. Li, W. Wu, M. Huang, H. S.-H. Chung, M. Liserre, and F. Blaabjerg, "Design of PWM-SMC controller using linearized model for grid-connected inverter with LCL filter," *IEEE Trans. Power Electron.*, vol. 35, no. 12, pp. 12773–12786, Dec. 2020.

[22] R. Ortega, A. Van Der Schaft, B. Maschke, and G. Escobar, "Interconnection and damping assignment passivity-based control of port-controlled Hamiltonian systems," *Automatica*, vol. 38, no. 4, pp. 585–596, 2002.

[23] Z. Liu, Z. Geng, S. Wu, X. Hu, and Z. Zhang, "A passivity-based control of Euler–Lagrange model for suppressing voltage low-frequency oscillation in high-speed railway," *IEEE Trans. Ind. Informat.*, vol. 15, no. 10, pp. 5551–5560, Oct. 2019.

[24] J. Li, M. Wang, J. Wang, Y. Zhang, D. Yang, J. Wang, and Y. Zhao, "Passivity-based control with active disturbance rejection control of Vienna rectifier under unbalanced grid conditions," *IEEE Access*, vol. 8, pp. 76082–76092, 2020.

[25] J. Zhao, W. Wu, Z. Shuai, A. Luo, H. S.-H. Chung, and F. Blaabjerg, "Robust control parameters design of PBC controller for LCL-filtered grid-tied inverter," *IEEE Trans. Power Electron.*, vol. 35, no. 8, pp. 8102–8115, Aug. 2020.

[26] Y. Chen, M. Wen, and E. Lei, "Passivity-based control of cascaded multilevel converter based D-statcom integrated with distribution transformer," *Electr. Power Syst. Res.*, vol. 154, pp. 1–12, Jan. 2018.

[27] J. Min, F. Ma, Q. Xu, Z. He, A. Luo, and A. Spina, "Analysis, design, and implementation of passivity-based control for multilevel railway power conditioner," *IEEE Trans. Ind. Informat.*, vol. 14, no. 2, pp. 415–425, Feb. 2018.

[28] J. Lai, X. Yin, Z. Zhang, Z. Wang, Y. Chen, and X. Yin, "System modeling and cascaded passivity based control for distribution transformer integrated with static synchronous compensator," *Int. J. Electr. Power Energy Syst.*, vol. 113, pp. 1035–1046, Dec. 2019.

[29] X.-H. Liang, K. Yamada, N. Sakamoto, and I. Jikuya, "Model predictive controller design to suppress rate-limiter-based pilot-induced oscillations," *Trans. Jpn. Soc. Aeronaut. Space Sci.*, vol. 49, no. 166, pp. 239–245, 2007.

[30] M. Huang, X. Wang, P. C. Loh, and F. Blaabjerg, "LLCL-filtered grid converter with improved stability and robustness," *IEEE Trans. Power Electron.*, vol. 31, no. 5, pp. 3958–3967, May 2016.

[31] J. Zhao, C. Xie, K. Li, J. Zou, and J. M. Guerrero, "Passivity-oriented design of LCL-type grid-connected inverters with Luenberger observer-based active damping," *IEEE Trans. Power Electron.*, vol. 37, no. 3, pp. 2625–2635, Mar. 2022.

[32] X. Wang, Y. He, D. Pan, H. Zhang, Y. Ma, and X. Ruan, "Passivity enhancement for LCL-filtered inverter with grid current control and capacitor current active damping," *IEEE Trans. Power Electron.*, vol. 37, no. 4, pp. 3801–3812, Apr. 2022.

[33] L. Harnefors, R. Finger, X. Wang, H. Bai, and F. Blaabjerg, "VSC input-admittance modeling and analysis above the Nyquist frequency for passivity-based stability assessment," *IEEE Trans. Ind. Electron.*, vol. 64, no. 8, pp. 6362–6370, Aug. 2017.

MIN HUANG (Member, IEEE) received the M.S. degree in electrical engineering from Shanghai Maritime University, Shanghai, China, in 2012, and the Ph.D. degree from the Institute of Energy Technology, Aalborg University, Aalborg, Denmark, in 2015. She is currently a Faculty Member with Shanghai Maritime University. Her research interests include power quality and control and power converters for renewable energy systems.

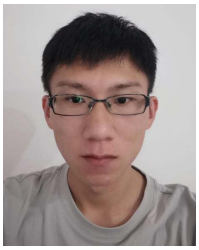

ZHICHENG ZHANG was born in Anhui, China, in 1996. He received the B.S. degree in electrical engineering from the Liaoning University of Technology, Liaoning, China, in 2019. He is currently pursuing the M.S. degree in electrical engineering with Shanghai Maritime University, Shanghai, China. His current research interests include sliding mode control, digital control techniques, and renewable energy generation systems.

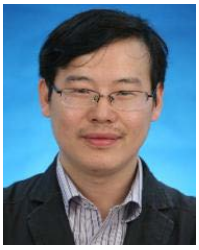

WEIMIN WU (Member, IEEE) received the Ph.D. degree in electrical engineering from the College of Electrical Engineering, Zhejiang University, Hangzhou, China, in 2005. He worked as a Research Engineer with the Delta Power Electronic Center (DPEC), Shanghai, from July 2005 to June 2006. Since July 2006, he has been a Faculty Member with Shanghai Maritime University, where he is currently a Full Professor with the Department of Electrical Engineering. He was a Visiting Professor with the Center for Power Electronics Systems (CPES), Virginia Polytechnic Institute and State University, Blacksburg, USA, from September 2008 to March 2009. From November 2011 to January 2014, he was also a Visiting Professor with the Department of Energy Technology, Aalborg University, Demark, working with the Center of Reliable Power Electronics (CORPE). He has coauthored over 100 papers and holds eight patents. His research interests include power converters for renewable energy systems, power quality, smart grid, and energy storage technology. He serves as an Associate Editor for the IEEE TRANSACTIONS ON INDUSTRIAL ELECTRONICS.

ZHILEI YAO (Senior Member, IEEE) was born in Jiangsu, China. He received the B.S., M.S., and Ph.D. degrees in electrical engineering from the Nanjing University of Aeronautics and Astronautics, Nanjing, China, in 2003, 2006, and 2012, respectively.

From 2003 to 2019, he was with the Yancheng Institute of Technology. In 2020, he joined the Shanghai Maritime University, Shanghai, China, where he is currently a Professor in electrical engineering. He was a Visiting Scholar with the Department of Energy Technology, Aalborg University, from 2014 to 2015. He holds more than 50 patents, and has authored or coauthored of more than 90 technical papers. His current research interests include DC–DC converters, inverters, and distributed power generation.

Dr. Yao is an Associate Editor of IEEE ACCESS.